A level set approach for the analysis of flow and compaction during resin infusion in composite materials

Joaquim Vilà , Carlos González , Javier LLorca

A B S T R A C T

Fluid flow and fabric compaction during vacuum assisted resin infusion (VARI) of composite materials was simulated using a level set-based approach. Fluid infusion through the fiber preform was modeled using Darcy's equations for the fluid flow through a porous media. The stress partition between the fluid and the fiber bed was included by means of Terzaghi's effective stress theory. Tracking the fluid front during infusion was introduced by means of the level set method. The resulting partial differential equations for the fluid infusion and the evolution of flow front were discretized and solved approximately using the finite differences method with a uniform grid discretization of the spatial domain. The model results were validated against uniaxial VARI experiments through an $[0]_8$ E-glass plain woven preform. The physical parameters of the model were also independently measured. The model results (in terms of the fabric thickness, pressure and fluid front evolution during filling) were in good agreement with the numerical simulations, showing the potential of the level set method to simulate resin infusion.

1. Introduction

VARI (vacuum assisted resin infusion) is an open mould process that uses vacuum as driving force to infiltrate resin through bagged fiber preform. One mould face is replaced by a vacuum bag, leading to reduced tooling costs but increasing the complexity of the infiltration process from the viewpoint of the control of final thickness and porosity. Research activities in recent years were focussed in understanding the physical mechanisms of infiltration including fluid flow, compaction and curing to overcome these limitations. The final goal was to develop simulation tools that can predict accurately the VARI process (see, for instance, Correia et al. [3], Šimáček et al. [14,13], Michaud and Mortensen [9], Trochu et al. [17], Joubaud et al. [7], Modi et al. [10]).

The infiltration and the associated thickness changes during infusion are a consequence of the stress partition between the infused resin and the fiber preform. Before infusion, the atmospheric pressure is transmitted to the mould through the fiber bed skeleton. Part of the load carried by the fibers is transferred to the infused resin, leading to a spring-back of the fiber preform with the corresponding increase in thickness, which continues until the fluid front reaches the outlet gate and the steady-state regime is attained. However, the changes in the compaction of the fiber bed during infiltration modify the permeability and the infiltration velocity. As a result, the pressure gradient in the liquid along the infiltration direction is not constant and depends on a complex interaction among permeability, fiber compaction and the stress partition between the fluid resin and the fiber bed. The relevant strategies for the analysis of resin infusion were reviewed by Correia et al. [3] and apply simultaneously Terzaghi's effective stress theory to model the stress partition and Darcy's and continuity equations to simulate the fluid flow. The fabric compressibility introduces additional difficulties with respect to the constant thickness case (standard resin transfer moulding using two rigid moulds) which are taken into account by formulating the continuity equation in the deformed control volume of the material.

This analysis strategy gives rise to a non-linear partial differential equation for the pressure field which can be solved with the appropriate boundary and initial conditions at the inlet and outlet resin gates. The pressure field is controlled by the permeability and compressibility of the fiber bed which varies with the fiber volume fraction according to the local stress partition. However, the solution of the infusion problem has to take into account that the infiltration front evolves during the filling stage from the inlet to the outlet gate until the total saturation of the fiber preform. Therefore, the partial differential equation for the pressure field,

valid only for the fully saturated media, should be solved with a moving boundary condition, namely the flow front, during filling. Several strategies have been developed to track the flow front position in injection/infusion problems, including the explicit updating of the flow front based on Darcy's average fluid velocity or the control volume algorithm developed by Bruschke and Advani [1]. Within this context, the level set method [11,12] has emerged as an efficient tool to solve moving boundaries problems in multiphysics and was successfully applied to study crystal growth and solidification [2] and fluid flow [16], among various problems. The method is based on the development of an evolving level set function controlled by a Hamilton–Jacobi differential equation matching its zero level with the evolving flow front. The level set equation is used to separate two media (i.e. dry and wet regions during infusion/injection) with different properties, which are taken into account into the conservation equations of fluid flow.

The level set approach is used in this investigation to study fluid flow and fabric compaction during resin infusion of composite materials. The model was developed for multidimensional flow although the experimental validation was carried out for unidimensional in-plane flow through a porous fiber preform (standard VARI process without distribution media) for simplicity. To this end, infusion tests were carried out and the out-of-plane displacements of the vacuum bag during the filling and post-filling stages were measured by digital image correlation while the fluid pressure at different locations was provided by pressure transducers. All the physical properties of the fluid and the fiber bed (permeability, viscosity as well as the relationship between the fiber bed compaction pressure and the fiber volume fraction under dry and wet conditions) were determined from independent tests. The experimental set-up as well as the results of the infusion experiments are presented in Section 2, followed by the tests to measure the fabric permeability and fiber bed compaction. The level-set model to simulate the infiltration process is detailed in Section 3, while Section 4 presents the comparison of the experimental data with the model predictions in terms of the vacuum bag compaction displacements and resin pressure evolution. The potential of the level set approach to simulate resin infusion in composite materials is clearly demonstrated.

2. Experimental results

2.1. Infusion tests

Vacuum infusion was carried out through an eight ply E-glass plain woven fabric. Fabric strips of length $L = 250$ mm and width $B = 80$ mm were cut and placed on an PMMA tool surface previously coated with a release agent using a $[0^\circ]_8$ lay-up configuration. The fiber preform was covered with a standard vacuum bag (5 μm NBF-540-LFT) and the whole set was sealed with standard tacky tape (LTT-90B). Resin inlet and outlet were connected to the fluid pot and the vacuum pump, respectively, with a rigid tube of 12 mm in diameter.

A blend of corn syrup (70%) and water (30%) was used as infusion fluid. The blend was degassed immediately before the infiltration for 20 min using a vacuum container. The viscosity of the fluid was measured with a rotational viscosimeter Fungilab with L2 type spindle at 30 rpm at ambient temperature. No shear strain rate effects were taken into account and the fluid is assumed to exhibit a Newtonian behavior. The viscosity of the corn syrup blend at ambient temperature is reported in Table 1. Fabric properties (porosity, areal and fiber density) can also be found in this table.

The fluid pressure during infusion was monitored with three pressure transducers (Omega PX61V0-100AV) equally distributed over the length of the infusion strip at 25%, 50% and 75% of its length. The transducers were inserted in the mould through cylindrical cavities, Fig. 1. The outlet vacuum was controlled with a screw-driven valve regulator (TESCOM DV) while a pressure transducer (HBM P8AP) was used to monitor the current vacuum pressure, p_{vac}. The out-of-plane displacement field due to changes in the fabric compaction, $h(x,t)$ in Fig. 1, was continuously measured by means of the digital image correlation using the software VIC-3D [18]. To this end, a speckle pattern was created on the vacuum side of the bag by spraying white paint followed by the dispersion of fine black dots. Two high resolution digital cameras were placed as shown in Fig. 1 and 29 Mpixels images were acquired with both cameras at a rate of 10 images per minute. Digital image correlation was only performed within a specific area of interest (AOI) of length $L_{AOI} = 0.21$ m and width $B_{AOI} = 0.01$ m. The reference geometry was given by the vacuum bag surface after the application of some debulking cycles to minimize distortions due to the nesting of individual fabric yarns.

Table 1
Fluid viscosity and fiber preform properties.

Viscosity μ (Pa s)	2.35
Fabric porosity (%)	0.48
Areal density σ_f (kg/m^2)	0.49–0.51
Fiber density ρ_f (kg/m^3)	2540

The evolution of the vacuum bag thickness with time at different positions (located at 10%, 32%, 50%, 70% and 90% along the infusion line within the AOI) obtained by digital image correlation is shown Fig. 2. The initial thickness of the $[0^\circ]_8$ fabric after the application of the debulking cycles was ≈2.8 mm. A slight reduction of the local thickness was detected as soon as the fluid entered into the bag, which is usually attributed to fluid lubrication of the fiber bed at the flow front. Afterwards, the bag thickness increased continuously due to the stress transfer between the fiber bed and the infusion fluid. The external load induced by the atmospheric pressure, initially supported by the fiber bed skeleton, was progressively transferred to the fluid leading to a spring-back effect with the corresponding increase of the fabric thickness. The pressure build-up in the fluid was recorded by the transducers and is plotted in Fig. 3. The pressure increase is very fast as soon as the fluid reaches the corresponding position and rapidly attains an asymptotic value once the steady state regime is established and the whole fabric is filled by the fluid. Lubrication and spring-back effects during infiltration were also reported by other authors [19,4]. The inlet gate was closed at $t \approx 8000$ s, once the flow front reached the outlet gate, and the steady-state regime was attained. This leads to a progressive homogenization of the thickness within the infused area in the post filling stage, accompanied by a reduction in the fluid pressure as the load is transferred back to the fiber bed. The experiments were finished at $t \approx 10,000$ s.

The shape of the vacuum bag at different instants during the filling stage is shown in Fig. 4(a). The contour plot of the increment in the fabric thickness, $\Delta h(x,t)$, obtained by digital image correlation, is also plotted in Fig. 4(b) for the same infusion times. Both figures show that digital image correlation captures very accurately the progression of the fluid along the infusion length, which increases continuously until the fluid front reached the outlet gate and the fabric was completely saturated. Very interestingly, digital image correlation was able to capture the roughness of the plain woven fabric (tow width of ≈5 mm).

In fact, the information provided by digital image correlation allowed the determination of the flow front position even if the direct optical observation of the fabric was not possible due to the speckle pattern. According to the results showed in Fig. 2, the thickness of the fabric initially decreased due to the lubrication of the fiber-to-fiber contacts and then increased as a result of the

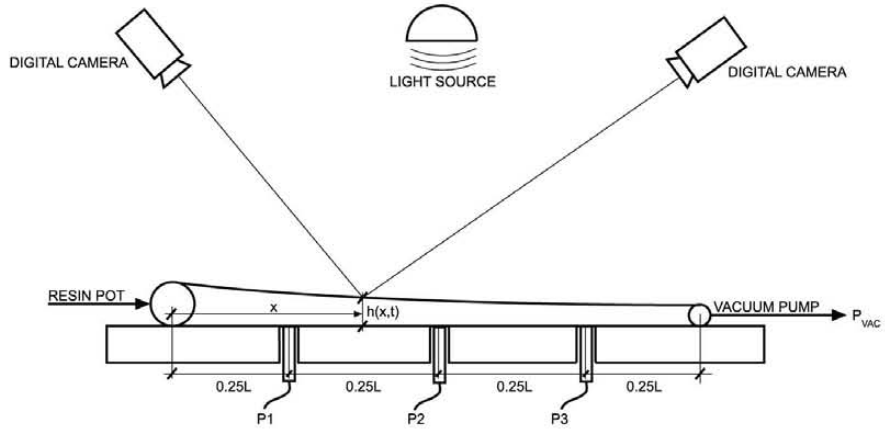

Fig. 1. Experimental infusion set-up. The location of the three pressure transducers and the sketch of the digital image correlation system are shown.

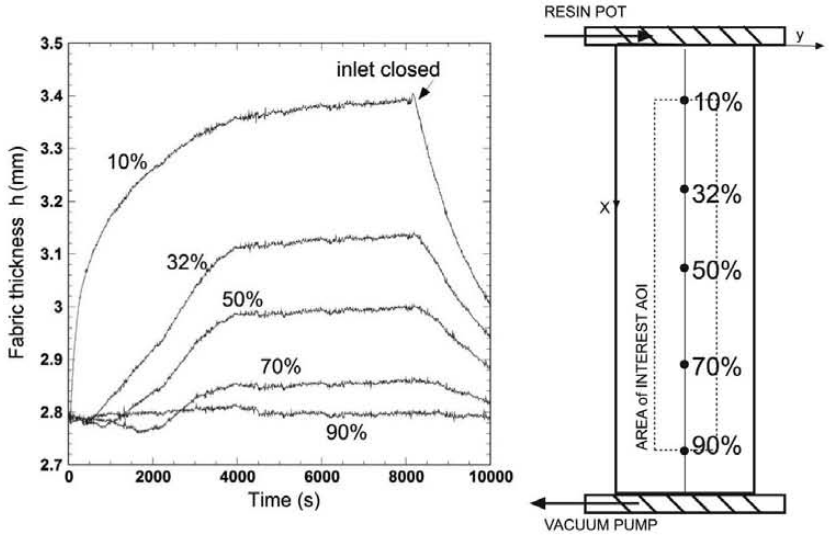

Fig. 2. Evolution of the vacuum bag thickness with time during infusion at different positions of the strip located within the AOI at 10%, 32%, 50%, 70% and 90% along the infusion line.

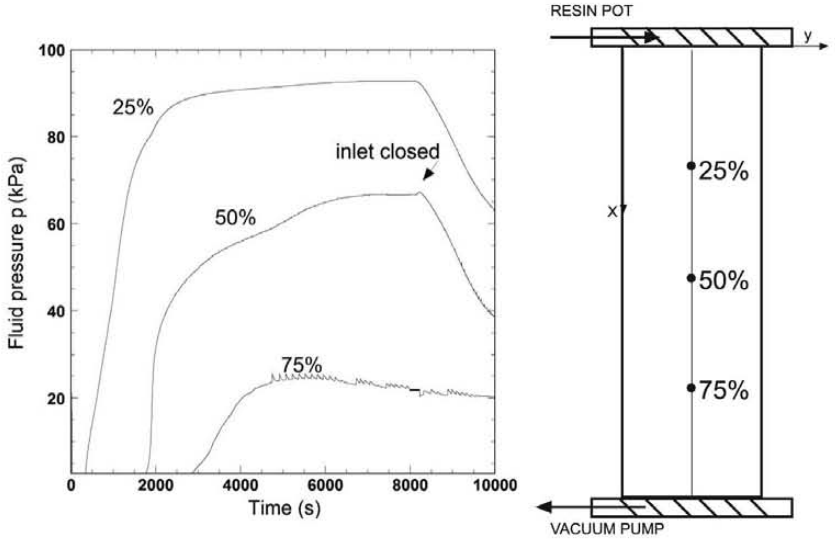

Fig. 3. Evolution of the fluid pressure at different positions of the strip located at 25%, 50% and 75% along the infusion line.

load transfer between the fluid and the fiber bed. The transition point between both phenomena (attained when the bag thickness reached zero after the initially reduction due to lubrication) was used to track the actual position of flow front during infiltration. Following this assumption, the location of flow front with time is plotted in Fig. 5.

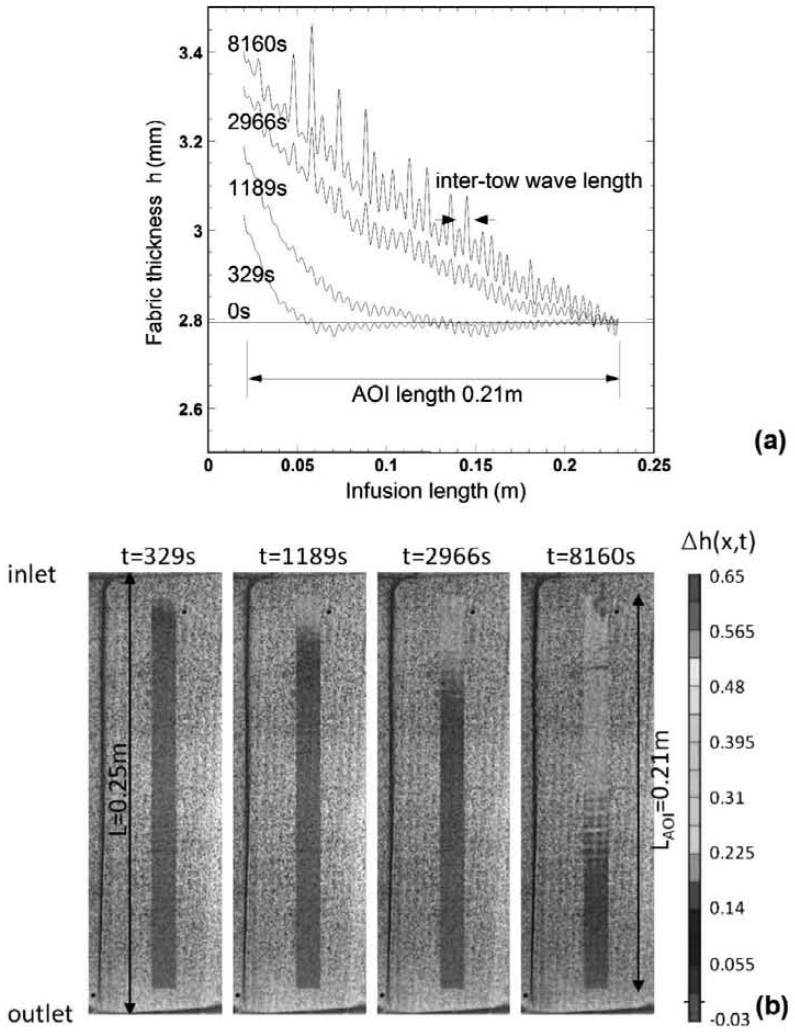

Fig. 4. (a) Evolution of the bag thickness profile along the infusion length within the AOI for different infusion times. (b) Contour plot of the increment in the fabric thickness, $\Delta h(x,t)$, within the AOI for different infusion times. (For interpretation of the references to color in this figure legend, the reader is referred to the web version of this article.)

2.2. Permeability

The in-plane permeability of the $[0°]_8$ fabric and its dependence with the fiber volume fraction was measured using a standard closed work cell with controlled fabric thickness. The experimental set-up is sketched in Fig. 6(a) and is similar to fixtures proposed by other authors Stadtfeld et al. [15], Yenilmez et al. [20]. The closed mold contains one face machined in transparent PMMA which allows the visual inspection of the flow during the experiments. The inlet pressure, p_0, is increased in several steps (0.25, 0.5, 0.75 and 1.0 atm) while the outlet is maintained at atmospheric pressure, p_{atm}. The fluid flow rate (obtained from the fluid mass and density) of the corn syrup blend was measured for each imposed pressure gradient. The mould was coupled to an electromechanical testing frame which allowed a precise control of the fiber volume fraction (fabric thickness in the closed mold h in Fig. 6(a) during the tests). All the experiments were carried out under fluid saturated conditions using different thicknesses corresponding to fiber volume fractions in the range 40–60%. The evolution of the in-plane fabric permeability, K_i, with the fiber volume fraction, V_f, is plotted in Fig. 6(b). The experimental results followed the Carman-Kozeny equation Gutowski et al. [5],

$$K_i = k_{i0}\frac{(1-V_f)^3}{V_f^2} \quad (1)$$

where k_{i0} is an empirical constant which depends on the specific fiber bed architecture. It was obtained by the least squares fitting of the experimental results in Fig. 6(b) and can be found in Table 2.

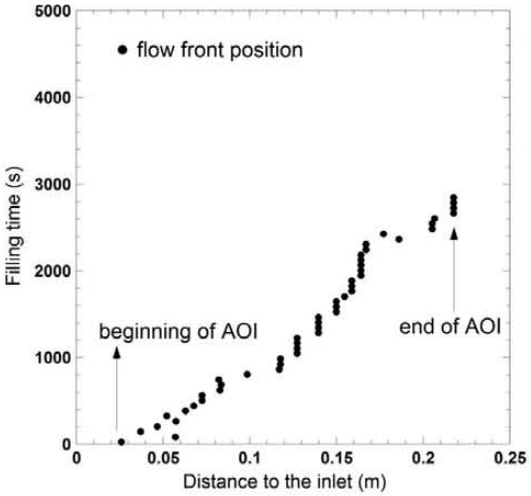

Fig. 5. Evolution of the flow front position with filling time.

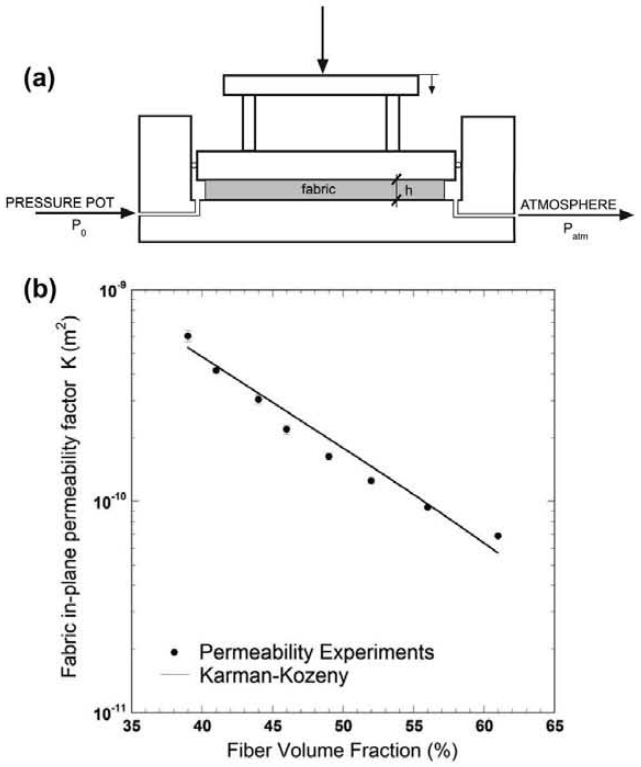

Fig. 6. (a) Sketch of the experimental set-up for the in-plane permeability tests. (b) Evolution of the in-plane fabric permeability, K_i, with the fiber volume fraction, V_f.

2.3. Compaction

Rectangular fabric laminates of 100 × 250 mm² and $[0^\circ]_8$ lay-up configuration were prepared following the procedure described for the infusion experiments to measure the fiber compaction. The speckle pattern was applied to the upper surface and tests were carried out by loading and unloading the fiber preform with a controlled vacuum pressure gage. The profile of the bagged surface was measured by digital image correlation after several seconds of stabilization. It was assumed that the pressure gradient inside the bag was negligible and the gage pressure supported by the fibers was homogeneously distributed throughout the fabric preform [4]. Experiments were carried out under dry and wet conditions in order to characterize the material during the filling and post-filling states of the infusion [21], Yenilmez et al. [20]. To this end, the fabric was impregnated with the corn syrup blend prior to the bagging operation. The evolution of the fiber volume fraction with the fiber compaction pressure, p_{fiber}, is presented in Fig. 7 for both dry and wet conditions. Each point in this figure corresponds to the fiber volume fraction obtained from the average value of h and the error bars stand for the standard deviation of h throughout the fabric surface. The higher volume fraction under wet conditions for the same applied pressure is usually attributed to nesting effects.

The experimental evolution of the fiber volume fraction with the fiber compaction pressure was used to fit a power law by the least squares method, according to Correia et al. [3]

Table 2
Permeability and compaction parameters of the $[0^\circ]_8$ E-glass fabric.

k_{i0} (m^2)	3.67×10^{-10}	
a (%/Pa)	Dry: 48.98	Wet: 44.64
b	Dry: 0.0285	Wet: 0.0637

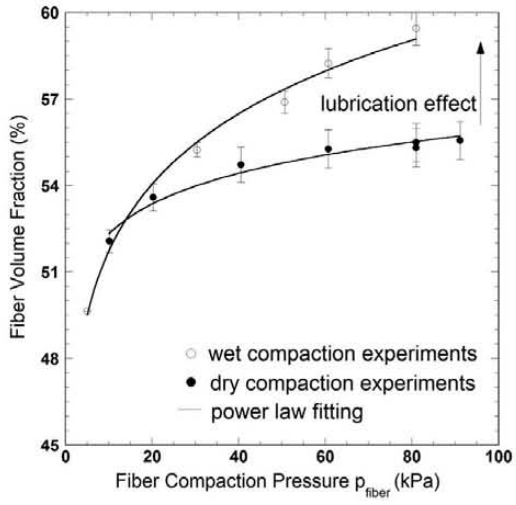

Fig. 7. Evolution of the fiber volume fraction as a function of the applied pressure under dry and wet conditions in the fiber compaction experiments.

$$V_f = a p_{fiber}^b \tag{2}$$

where b is the stiffening index, and a the fiber volume fraction for 1 Pa of applied pressure. The corresponding values of a and b for dry and wet conditions can be found in Table 2.

3. A level set model of infusion

The model is based on the resolution of the Darcy's equations for the fluid flow through a porous media. Darcy's equation establishes a linear relationship between the average fluid velocity through the fiber preform, $\mathbf{v}$, and the externally imposed pressure gradient, ∇p. The proportionality factor is related with the fabric permeability tensor $\mathbf{K}$ and the fluid viscosity μ according to,

$$\mathbf{v} = -\frac{\mathbf{K}}{\mu}\nabla p \tag{3}$$

The fabric deformability during infusion should be taken into account and this is carried out through the mass conservation law according to

$$\rho \nabla \cdot \mathbf{v} + \frac{\partial \rho}{\partial t} = 0 \tag{4}$$

where ρ is the current density of the infused material within the volume considered. Assuming that the compaction takes place in the through-the-thickness direction of the fabric (normal compaction), the conservation law can be expressed in terms of the change in the fiber volume fraction as, Šimáček [14]

$$\nabla \cdot \mathbf{v} = \frac{1}{V_f}\frac{\partial V_f}{\partial t} \tag{5}$$

The partial differential equation for the pressure field evolution $p(\mathbf{x}, t)$ can be obtained from Eqs. (3) and (4) as

$$\nabla\left(\frac{\mathbf{K}}{\mu}\cdot\nabla p\right) = -\frac{1}{V_f}\frac{\partial V_f}{\partial t} \tag{6}$$

In addition, the stress partition between the fiber bed, p_{fiber}, and the infusion fluid, p, is established by means of the Terzaghi's effective stress theory according to

$$p_{fiber} = p_{atm} - p \tag{7}$$

where p_{atm} is the atmospheric pressure in the case of vacuum infusion. The fiber volume fraction, V_f, is also pressure dependent so the final thickness of the composite will depend on the pressure

transferred from the resin to the fiber preform and, therefore, $V_f = V_f(p_{atm} - p)$. Similarly, the permeability tensor, $\mathbf{K}$, is a function of the fiber volume fraction, leading to a non-linear partial differential equation for the pressure field given by

$$\nabla\left(\frac{\mathbf{K}(V_f)}{\mu}\cdot\nabla p\right) = -\frac{\partial V_f/\partial p}{V_f}\frac{\partial p}{\partial t} \tag{8}$$

where the physical parameters in this equation (namely, the fiber bed compressibility, $V_f(p_{fiber})$, the in-plane permeability of the fabric, $\mathbf{K}(V_f)$, and the fluid viscosity, μ) were measured in Section 2 for the system under consideration.

Eq. (8) is only valid when the fluid completely fills the solution domain. This is not the case, however, of infusion because the fluid front evolves naturally during the process as the fluid moves through the dry preform. Thus, a strategy has to be developed to deal with this scenario. In the level set method, the fluid front is defined with the aid of a function $\phi(\mathbf{x}, t)$, which stands for the distance of point $\mathbf{x}$ to the flow front at time t [11]. Obviously, the flow front is identified by the condition $\phi(\mathbf{x}, t) = 0$ and tracking the fluid front is equivalent to find the zero level of the evolving function ϕ during infusion. Differentiating the former expression and using the chain rule, the initial value problem for the level set function can be obtained as

$$\frac{\partial\phi}{\partial t} + \frac{\partial\phi}{\partial\mathbf{x}}\frac{\partial\mathbf{x}}{\partial t} = \frac{\partial\phi}{\partial t} + F|\nabla\phi| = 0 \tag{9}$$

where F is the velocity normal to the fluid front (tangential velocities do not move the fluid front), which can be obtained from Eq. (3) with the permeability that changes following the Carman-Kozeny Eq. (1).

Eq. (8) can be modified by the level set function to indicate whether or not the region is filled by the fluid according to

$$H(\phi)\nabla\left(\frac{\mathbf{K}(p)}{\mu}\nabla p\right) = -\frac{\partial V_f/\partial p}{V_f}\frac{\partial p}{\partial t} \tag{10}$$

where $H(\phi)$ is a step shape function whose value is equal to 1 in the regions filled with fluid ($\phi < 0$) and zero in the dry regions ($\phi > 0$), Fig. 8. Thus, according to Eq. (10), $p = p_{vac}$ in the dry region. $H(\phi)$ has to be smoothed out in a narrow transition zone around the fluid front in order to avoid numerical problems during the integration of the partial differential equation. In this case,

$$H(\phi) = (1 + e^{-\alpha\phi})^{-1} \tag{11}$$

where α ($\gg 1$) is the parameter controlling the width of the transition region.

3.1. Numerical strategy and discretization

Eqs. (10) and (9) have to be solved simultaneously within the 2D domain corresponding to the rectangular fabric of dimensions $L \times B$ using the finite differences method, Fig. 8. The spatial domain is discretized using a uniform grid (i,j) with equally spaced increments Δx and Δy. The first and second order spatial derivatives arising from Darcy's Eq. (10) are approximated with the central differences scheme while the time derivatives in the same equation are discretized with a standard forward Euler method using Δt as time increment.

The level set Eq. (9) is hyperbolic and it can be solved by a combination of the forward Euler scheme for the time discretization and the upwind spatial algorithm for the spatial discretization [11]. Mathematically,

$$\phi_{ij}^{n+1} = \phi_{ij}^{n} - \Delta t[\max(F_{ij}, 0)\nabla^{+} + \min(F_{ij}, 0)\nabla^{-}] \tag{12}$$

where ϕ_{ij}^{n} is the current level set value at the local position i,j and time t, ϕ_{ij}^{n+1} the prediction for the incremented time $t + \Delta t$ and F_{ij} stands for the flow front velocity at the local position i,j and time t. The upwind operators read as follows

$$\nabla^{+} = [\max(D_{ij}^{-x}, 0)^2 + \min(D_{ij}^{x}, 0)^2 + \max(D_{ij}^{-y}, 0)^2 + \min(D_{ij}^{y}, 0)^2]^{1/2} \tag{13}$$

$$\nabla^{-} = [\max(D_{ij}^{x}, 0)^2 + \min(D_{ij}^{-x}, 0)^2 + \max(D_{ij}^{y}, 0)^2 + \min(D_{ij}^{-y}, 0)^2]^{1/2} \tag{14}$$

where $D_{ij}^{x} = (\phi_{i+1,j}^{n} - \phi_{ij}^{n})/\Delta x$ and $D_{ij}^{-x} = (\phi_{ij}^{n} - \phi_{i-1,j}^{n})/\Delta x$ stand for the forward and backward first order operators, respectively, for the x-direction spatial derivatives (the same definitions correspond to the y-direction spatial derivatives).

The stable time increment Δt should satisfy the Courant-Friedreichs-Lewy stability condition, which is given by

$$\max(F\Delta t) \leqslant \Delta x, \Delta y \tag{15}$$

From a practical viewpoint, a time increment is assumed *a priori* on the basis of previous experience.

It should be noticed that nothing guarantees that the updated level set function ϕ_{ij}^{n+1}, Eq. (12), provides the actual distance of each point to the flow front and this can generate convergence problems after a few time increments. To avoid this problem, several reinitialization schemes for the level set function after each time increment were proposed in the literature [16,6] based on resolution of the following standard differential equation

$$\frac{\partial\phi}{\partial\tau} = S(\phi_0)\left(1 - \sqrt{\left(\frac{\partial\phi}{\partial x}\right)^2 + \left(\frac{\partial\phi}{\partial y}\right)^2}\right) \tag{16}$$

$$\phi(\mathbf{x}, \tau = 0) = \phi_0(\mathbf{x}) \tag{17}$$

where $\phi_0(\mathbf{x})$ is the actual location of the fluid front, S is the sign function (that is usually smoothed-out to $S(\phi_0) = \phi_0/\sqrt{\phi_0^2 + \epsilon^2}$ with ϵ a small positive number due to numerical reasons), and τ a fictitious time. Obviously, the updated level set function will provide the distance of each point to the flow front given by $\phi_0(\mathbf{x})$.

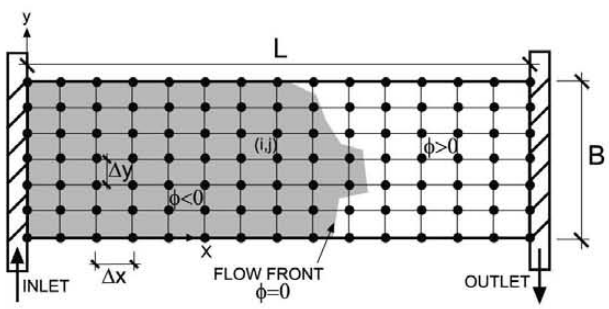

Fig. 8. Simulation domain for the level set method.

4. Results and discussion

The model described above was programmed in Matlab [8] and used to simulate the infusion experiments presented in Section 2. The rectangular fabric strip was discretized with an uniform grid with Δx = 3.125 mm and Δy = 2 mm to capture the evolution of the flow front during the experiments. Initial and boundary conditions were imposed on the rectangular domain, Fig. 8. The initial pressure was zero everywhere (the vacuum pressure). The boundary conditions at the four edges of the rectangular domain were the following: the pressure was set to zero (vacuum pressure) at the outlet ($x = L$) while the fluid inlet pressure at $x = 0$ was rapidly raised from zero to p_0 (atmospheric pressure) using a exponential

function $p(x=0,z,t)=p_0(1-e^{-At})$, where A is small. This boundary condition simulates the inlet opening operation. Finally, fluid flow at $y=0$ and $y=B$ has to be parallel to the longitudinal edges and, therefore, the spatial derivatives along the y direction were set to zero. This set of initial and boundary conditions leads to unidimensional flow along the x direction, in agreement with the experiments. The time increment was set to $\Delta t=0.01$ s to fulfill the stability condition, Eq. (15), during the analysis. The physical parameters of the model, including the fluid viscosity μ, in-plane fabric permeability $\mathbf{K}=\mathbf{K}(V_f)$ and fiber bed compressibility were also measured and can also be found in Section 2.

The model was run in two steps. The inlet pressure was first raised up to p_{atm} and maintained constant throughout the filling stage up to ≈8000 s. Afterwards, the inlet was closed and this condition of zero fluid velocity was introduced by imposing $\nabla p=0$ at the inlet ($x=0$). This boundary condition was maintained until the end of the analysis at $t\approx 10,000$ s.

The solution of the Eq. (10) provides the fluid pressure field p in the whole domain. The stress carried by the fibers was computed from Terzaghi's effective stress, Eq. (7), and the thickness change was obtained from the actual fiber volume fraction given by Eq. (2), where different coefficients are used for the dry or wet regions of the fabric. The experimental results of the evolution of flow front with time and of the fabric thickness at the various distances from the inlet are compared with the simulations in Fig. 9(a) and (b), respectively. The model captured accurately the advancement of the flow front with time and the changes in fabric thickness at the different locations as well as the magnitude of the fabric compaction during the filling and post-filling stages. After the flow front reaches an specific position, the fluid pressure builds up and the atmospheric pressure is shared with the fiber bed resulting in the corresponding thickness increase. Of course, the model was not able to capture the initial thickness reduction when the flow front reached a location because the lubrication effect (responsible for this behavior) was not accounted for in the simulations but this phenomenon is of very limited importance.

The experimental results of the evolution of the fluid pressure with time at three different locations along the infusion length is compared with the simulations in Fig. 9(c). The agreement between both was also good: the fluid pressure was built-up rapidly after the flow front reached an specific location until a plateau value was attained. The atmospheric pressure was shared with the fiber bed, leading to the corresponding thickness increase, which varied with the fluid pressure. After the inlet gate is closed, the

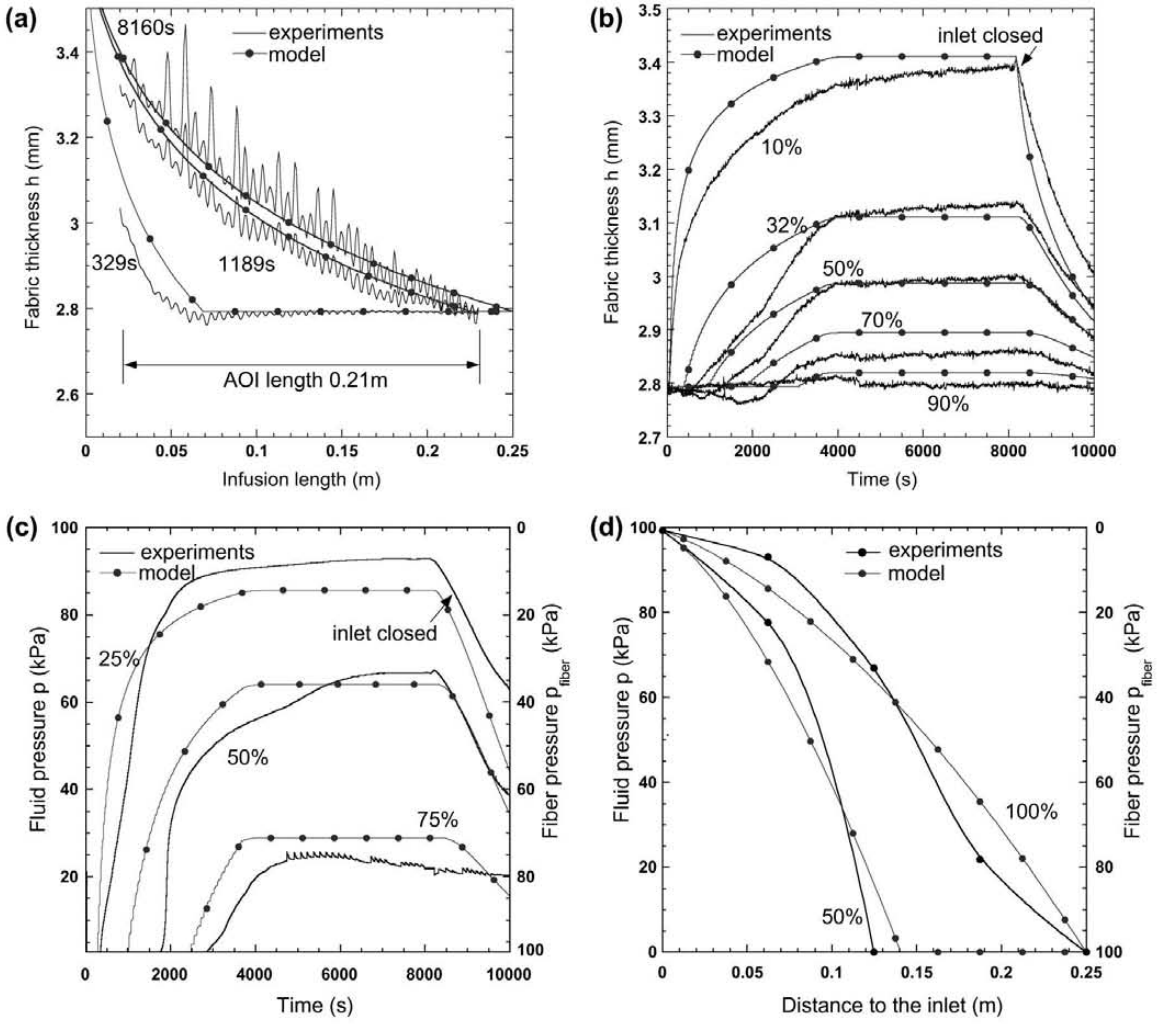

Fig. 9. Comparison between experimental and simulation results. (a) Evolution of the flow front with time along the AOI. (b) Evolution of the fabric thickness with time at different locations along the infusion length (10%, 32%, 50%, 70% and 90%). (c) Evolution of the fluid pressure at at different locations along the infusion length (25%, 50% and 75%). (d) Pressure profile along panel length when the flow front reached 50% (t = 1189 s) of the fabric length, and when the inlet is closed (t = 8160 s). The stress carried by the fiber bed, p_{fiber}, according to Eq. (7), is indicated in the right Y axis of (c) and (d). (For interpretation of the references to color in this figure legend, the reader is referred to the web version of this article.)

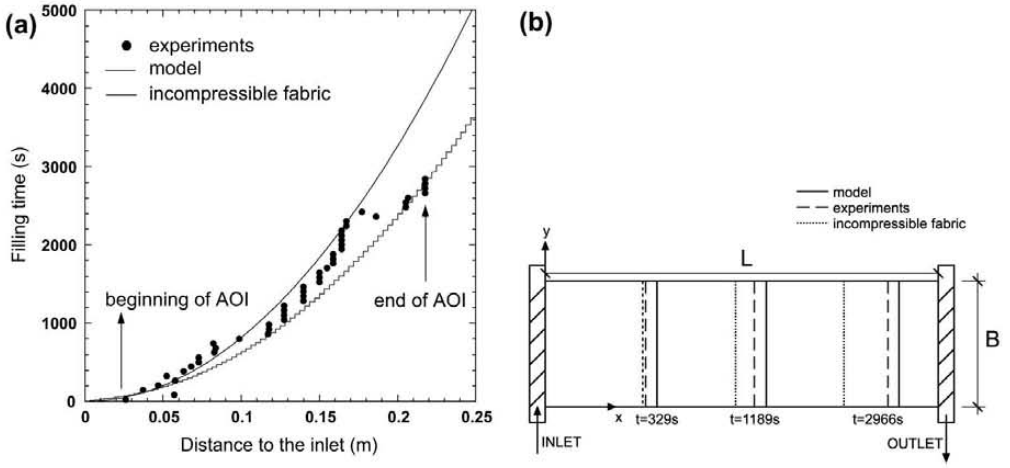

Fig. 10. (a) Comparison between experimental and simulation results of the filling time. (b) Experimental and simulation results of the solid–liquid interface in the *xy* plane for different filling times. The interface was always parallel to the *y* axis because flow was unidirectional along the *x* axis. (For interpretation of the references to color in this figure legend, the reader is referred to the web version of this article.)

fluid pressure within the bag is homogenized and the model also captured accurately this stage. The agreement is also good during the post-filling phase when the inlet gate is closed and the fluid pressure inside the bag is homogenized until a steady-state regime is attained. Small ripples and other irregularities found in the experimental curves were likely due to void movement and/or inhomogeneous fiber distribution.

Finally, the pressure profile along the infusion line obtained with the level set approach was compared with the experimental values recorded with the pressure transducers for filling times t = 1199 s and 8160 s, which correspond to the instants when the fluid front reached 50% of the fabric length and when the inlet is close, Fig. 9(d). The pressure profile along the infusion line was not linear due to the compressibility of the vacuum bag, as opposed to the incompressible case of standard RTM, in which the infusion between two rigid molds leads to a constant thickness.

The comparison between the experimental and numerical results of filling time is presented in Fig. 10(a). The agreement between both was excellent, showing a quadratic dependence with the distance to the inlet, as demonstrated in Correia et al. [3]. The results for the case of a rigid mould are also plotted for the sake of comparison. In this case, the fabric permeability does not change with the fluid pressure and Darcy's equation is simplified to $\partial^2 p/\partial x^2 = 0$ (linear pressure variation between inlet and outlet). The filling time can be easily determined by direct integration as $t_{fill} = (1 - V_f)\mu L^2/2Kp_{atm}$ and the results in Fig. 10 correspond to a fiber volume fraction of ≈60%. The longer filling times for the incompressible case are a result of the constant permeability of the fiber preform, which increased with time in the compressible case due to the fiber spring-back. The solid–liquid interface was always parallel to the *y* axis because flow was unidirectional along the *x* axis, Fig. 10(b).

5. Concluding remarks

A level set based model was developed to simulate the fluid flow and fabric compaction during VARI of composite materials. Fluid infusion through the fiber preform was modeled using Darcy's equations for the fluid flow through a porous media, including the continuity condition. The stress partition between the fluid and the fiber bed was included by means of Terzaghi's effective stress theory, leading to a non-linear partial differential equation. This equation is only valid in the infused region and its necessary to separate both regions. This was achieved by introducing a level set function ϕ in the partial differential equation which is defined at any given time as the distance to the flow front. Obviously, the flow front is identified by the condition $\phi = 0$ and tracking the fluid front is equivalent to finding the zero level of the evolving function during infusion by solving a hyperbolic partial differential equation.

The partial differential equations were discretized and solved approximately using the finite differences method with a uniform grid discretization of the spatial domain. Darcy's equation was solved using a standard Euler method for the time integration and a central differences algorithm for the spatial integration. The time integration of the level set equation was approximated with the forward Euler method while the upwind algorithm was used for the spatial integration to account for the hyperbolic nature of the evolution equation.

A 2D version of the model (that can be easily updated to 3D) was implemented in Mathlab. The model results were validated against uniaxial VARI infusion experiments through an $[0]_8$ E-glass plain woven preform. The evolution of the flow front and of the fabric thickness during infusion were measured by means of digital image correlation while the fluid pressure at various locations was monitored with pressure gages. The physical parameters of the model, including the fluid viscosity μ, in-plane fabric permeability $\mathbf{K} = \mathbf{K}(V_f)$ and fiber bed compressibility, were also independently measured. The model results (in terms of fabric thickness, pressure and fluid front evolution) were in good agreement with the experimental data, showing the potential of the level set method to simulate resin infusion. Future applications of the model will be devoted to study fluid infusion in 2D and 3D.

Acknowledgments

The experimental support of V. Martínez, J.L. Jiménez and M. de la Cruz is gratefully acknowledged.

References

[1] Bruschke M, Advani SG. A finite element/control volume approach to mold filling in anisotropic porous media. Polym Compos 1990;11(6):398–405.
[2] Chen S, Merriman B, Osher S, Smereka P. A simple level set method for solving stefan problems. J Comput Phys 1997;135(1):8–29.
[3] Correia N, Robitaille F, Long A, Rudd C, Šimáček P, Advani SG. Analysis of the vacuum infusion moulding process: I. Analytical formulation. Compos Part A: Appl Sci Manuf 2005;36(12):1645–56.
[4] Grimsley B, Pascal H, Xiaolan S, Cano R, Loss A, Byron PR. Flow and compaction during the vacuum assisted resin transfer moulding process. In: Int SAMPE Tech Conf 33; 2001. p. 141–53.
[5] Gutowski TG, Morigaki T, Cai Z. The consolidation of laminate composites. J Compos Mater 1987;21(2):172–88.

[6] Hartmann D, Meinke M, Schröder W. Differential equation based constrained reinitialization for level set methods. J Comput Phys 2008;227(14):6821–45.
[7] Joubaud L, Achim V, Trochu F. Numerical simulation of resin infusion and reinforcement consolidation under flexible cover. Polym Compos 2005;26(4):417–27.
[8] Matlab, version 7.10.0 (R2010a). Natick, Massachusetts: The MathWorks Inc.; 2010.
[9] Michaud V, Mortensen A. Infiltration processing of fibre reinforced composites: governing phenomena. Compos Part A: Appl Sci Manuf 2001;32(8):981–96.
[10] Modi D, Johnson M, Long A, Rudd C. Analysis of pressure profile and flow progression in the vacuum infusion process. Compos Sci Technol 2009;69(9):1458–64.
[11] Osher S, Sethian JA. Fronts propagating with curvature-dependent speed: algorithms based on Hamilton–Jacobi formulations. J Comput Phys 1988;79(1):12–49.
[12] Sethian J. Level set methods and fast marching methods: evolving interfaces in computational geometry, fluid mechanics, computer vision, and materials science. Cambridge monographs on applied and computational mathematics. Cambridge University Press; 1999.
[13] Šimáček P, Eksik O, Heider D, Gillespie JW, Advani SG. Experimental validation of post-filling flow in vacuum assisted resin transfer molding processes. Compos Part A: Appl Sci Manuf 2012;43:370–80.
[14] Šimáček P, Heider D, Gillespie JW, Advani SG. Post-filling flow in vacuum assisted resin transfer molding processes: theoretical analysis. Compos Part A: Appl Sci Manuf 2009;40:913–24.
[15] Stadtfeld HC, Erninger M, Bickerton S, Advani SG. An experimental method to continuously measure permeability of fiber preforms as a function of fiber volume fraction. J Reinf Plast Compos 2002;21(10):879–99.
[16] Sussman M, Smereka P, Osher S. A level set approach for computing solutions to incompressible two-phase flow. J Comput Phys 1994;114(1):146–59.
[17] Trochu F, Ruiz E, Achim V, Soukane S. Advanced numerical simulation of liquid composite molding for process analysis and optimization. Compos Part A: Appl Sci Manuf 2006;37(6):890–902.
[18] VIC-3D. Correlated solutions; 2010. <http://www.correlatedsolutions.com>.
[19] Williams C, Grove S, Summerscales J. The compression response of fibre-reinforced plastic plates during manufacture by the resin infusion under flexible tooling method. Compos Part A: Appl Sci Manuf 1998;29(12):111–4. selected papers presented at the fourth international conference on flow processes in composite material.
[20] Yenilmez B, Senan M, Murat Sozer E. Variation of part thickness and compaction pressure in vacuum infusion process. Compos Sci Technol 2009;69(11–12):1710–9.
[21] Yuexin D, Zhaoyuan T, Yan Z, Jing S. Compression responses of preform in vacuum infusion process. Chinese J Aeronaut 2008;21(4):370–7.